WILEY-VCH

Mechanically Reinforced Pseudo-Solid Polyelectrolyte Membranes Via Layer-by-Layer Assembly for High-Performing Lithium Metal Batteries

Bishnu P. Thapaliya[1*], *Babafemi Adigun*[2], *Tao Wang*[1], *Md Dipu Ahmed*[2], *Harry M. Meyer III*,[1] *Ivan Popov*[2,3], Sheng Dai[1,2*]

[1] Chemical Sciences Division, Oak Ridge National Laboratory, Oak Ridge, Tennessee 37831, United States

Email: prasadthapab@ornl.gov, dais@ornl.gov

[2] Department of Chemistry, The University of Tennessee, Knoxville, Tennessee 37996, United States

[3] The University of Tennessee – Oak Ridge Innovation Institute, University of Tennessee, Knoxville, Tennessee 37996, USA

Keywords: layer-by-layer (LbL) assembly, ionogel electrolyte, ionic liquids, polyanions, polycations, lithium metal batteries (LMBs)

Ionogels are emerging as high-potential pseudo-solid electrolytes for lithium metal batteries (LMBs), leveraging their intrinsic high ionic conductivity from entrapped ionic liquid (IL) electrolytes. However, their practical application has been hindered by poor mechanical strength stemming from the confinement of ILs within a polymer matrix. To address this challenge, we report the formation of conformal polyion coatings with functional groups relevant to LMBs application on ionogels, utilizing layer-by-layer (LbL) assembly strategy. This approach significantly enhances the mechanical strength (Young's modulus, tensile strength) and electrochemical performance of ionogels, owing to the tailored interface modifications introduced by functional groups specific conformal polyion coatings. The core of this methodology leverages the inherent ionic structure of ionogels to enable facile interface modification through coulombic interactions between polyanions and polycations. These conformally coated interface functionalized membranes show improved electrochemical performance when integrated with cathode materials such as $LiFePO_4$ (LFP) and $LiNi_{0.8}Mn_{0.1}Co_{0.1}O_2$ (NMC811) in a LMB configuration, underscoring their potential for robust, high-conductivity pseudo-solid membranes for LMB applications. These innovative pseudo-solid membranes offer improved mechanical and electrochemical properties, leading to higher battery efficiency and safety, making them promising candidates for next generation LMB technology.

1. Introduction

Lithium-ion batteries (LIBs) are indispensable for portable electronics and electric vehicles due to their high energy density and light weight.[1, 2] However, meeting the escalating energy demands of these devices requires overcoming significant challenges in current LIB technology, prompting extensive research into optimizing and designing LIBs to enhance capacity, power, safety, and stability.[3-5] Research efforts have focused on revitalizing Li-metal

as an anode material for developing high energy density lithium metal batteries (LMBs) due to its high theoretical capacity and low electrochemical potential, despite concerns over electrolyte instability and dendrite formation.[6-8]

To address safety issues associated with high-energy-density LMBs, solid-state electrolytes (SSEs) like polymeric glasses and crystalline ceramics have been explored for their stability across various temperatures and electrochemical potential for improved volumetric and gravimetric energy densities.[9-12] However, SSEs often suffer from low ionic conductivities at ambient temperatures, limiting their practical application in batteries.[13, 14] Improving the ionic conductivity, mechanical strength, electrochemical stability, and interfacial interactions of SSEs is crucial for enhancing battery performance.[11, 15-17] Researchers have investigated various types of solid electrolytes, including ceramic electrolytes known for their superior ionic conductivity but limited flexibility and high interfacial resistance[18-22], solid polymer electrolytes (SPEs) valued for their flexibility and ease of use despite moderate ionic conductivity[23-27], and hybrid solid electrolytes (HSEs) combining ceramics and polymers to improve mechanical strength and stability[28, 29]. The performance of SPEs is severely limited by their low ionic conductivity, as well as their mechanical strength and high resistance at the interfaces.[30-33]

Efforts to enhance the ionic conductivities and mechanical strength of SPEs have included strategies like incorporating ionic liquids (ionogel), organic solvents, and inorganic particles into polymer matrices.[28, 34-36] However, achieving both high ionic conductivity and mechanical strength remains a significant challenge, often requiring trade-offs. Layer-by-layer (LbL) assembly strategy could enhance the mechanical and electrochemical properties of polyelectrolyte membranes. LbL assembly involves sequentially depositing polycations and polyanions to create conformal and defect-free multilayer coatings, driven by entropic gain due to loss of counterions[37] or hydrogen bonding[17, 38], resulting in mechanically strong

membranes.[39, 40] This method allows precise control over membrane structure at the molecular level, facilitating the incorporation of extensive functional moieties.[41-47] LbL assembly strategy has been used to develop the membranes for different applications including solid-state electrolytes,[31, 32, 48, 49] fuel cells,[50] biomedical applications and drug delivery,[51-53] adhesive layers for cells,[54] nanocomposite materials[55] etc.

Herein, we report the development of highly charged polyelectrolyte membranes by alternatingly coating polyions with tailored functional groups on pendant chain onto a neutral ionogel membrane, leveraging the inherent ionic structure of the ionogel for facile interfacial modification. LbL assembly enables precise control over membrane structure at a molecular level, facilitating the integration of functional groups relevant to LMB applications. The resulting LbL polyelectrolytes demonstrate enhanced mechanical strength and electrochemical stability, making them promising for high-voltage applications. Our investigation reveals that the choice of functional moieties on the pendant groups significantly influences these properties. To further enhance the performance of LbL membranes, we introduced a scrubbing treatment to remove trapped counterions in the polymer matrix, using a high-concentration (approximately 5M) LiTFSI solution. This treatment significantly improves mechanical and electrochemical performance, albeit at the expense of ionic conductivity due to increased LiTFSI concentration and loss of ILs during scrubbing. After scrubbing, the LbL membrane (T-LPV) demonstrates enhanced electrochemical performance in LMB when paired with a LFP and NMC811 cathodes, showing promising charge/discharge capacities and cycling stability. LFP based LMB delivered stable capacity of ~142 mAh g^{-1} with a capacity retention (CR) of ~87%, corresponding to a decay rate of 0.03% per cycle with average CE of ~ 99.6 %. Similarly, NMC811 based LMB delivered high first charge-discharge capacity (233/208 mAh g^{-1}) with a CE of ~ 89% and retained a specific capacity of around 149.0 mAh g^{-1} with an average CE exceeding 99.9% after 85 cycles. These findings highlight the potential of LbL assembled

ionogels as robust pseudo-solid electrolytes for advancing solid-state LMB technologies towards commercial viability, offering higher battery efficiency and safety.

2. Results and Discussions

SPEs for LMBs must exhibit robust mechanical strength, high ionic conductivity, and a high lithium-ion transference number to effectively suppress the formation of lithium dendrites for smooth operation. While ionogels, which confine ionic liquids within a polymer matrix, achieve requisite ionic conductivities, they often sacrifice mechanical strength and lithium-ion transference number. In our previous work, we addressed this challenge using a LbL assembly approach, which significantly bolstered mechanical strength without compromising ionic conductivities.[31, 32] However, lower lithium-ion transport numbers observed in these structures led to increased polarization and dendritic lithium growth during battery cycling. The selection of polyion pairs, including the number of layers and surface properties, is critical for optimizing mechanical strength, ionic conductivity, and lithium-ion transference. We hypothesized that factors such as molecular weight, functional groups, pendant chains, and hydrogen bonding sites could further enhance one or more of these properties in coated membranes, in addition to Coulombic interactions. To investigate these parameters, three distinct polycations (PU, PV, PD) and two polyanions (PS, L) were selected based on their molecular weight, hydrogen bonding potential, pendant chains, and functional groups for ultrathin coatings on ionogel surfaces (**Figure 1a**). PU (molecular weight >10,000, amine and ether groups) and PD (molecular weight ~250,000, amine group) were selected for their hydrogen bonding sites, while PS (molecular weight ~1,000,000, aromatic and sulfonic groups), PV (molecular weight ~1,000,000, vinylpyrrolidone, methacrylate group, and pendant chain with a quaternary ammonium cation), and L (believed to have an ultra-high molecular weight, fluorinated and sulfonic groups) were chosen for their potential to enhance the mechanical and electrochemical properties of the membranes due to their high molecular weight and functional groups. The

neutral ionogel was coated with alternating conformal layers of polyanions (L or PS) and polycations (PV, or PD, or PU) via the LbL process (**Scheme 1**) that was driven either by entropic effects resulting from counterion loss or hydrogen bond interactions between polyions.[32, 37]

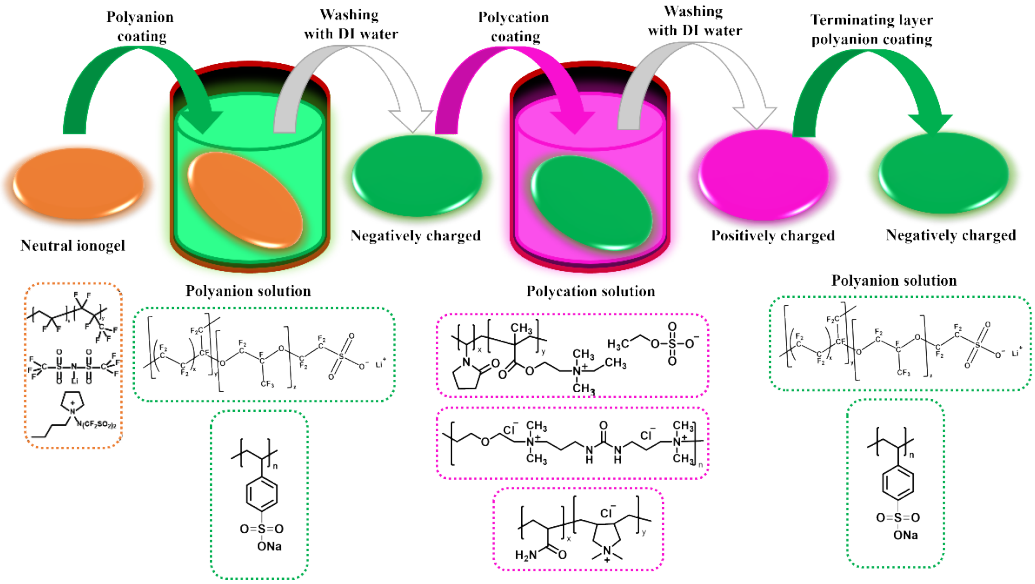

Scheme 1. Schematic representation of alternating conformal coating of polyanions (L or PS) and polycations (PV, or PD, or PU) on ionogel surface via LbL assembly approach.

The original ionogel electrolyte had low mechanical strength due to a large amount of ionic liquid in the polymer matrix. **Figure 1b** illustrates a substantial increase (~ 12-18 times) in tensile strength after LbL coating on ionogels with these ultrathin layers compared to the original ionogel (black curve, **Figure 1b**), highlighting the PV and LITHion as particularly effective due to their ultra-high molecular weight, ring structures, functional groups, and longer pendant chains, respectively. The enhanced mechanical strength of the membranes originates from the strong coulombic interactions and hydrogen bonding between polyions in the conformal coatings and the number of coated layers, which are absent in ionogel. The notable differences in tensile strength among the coated membranes arise from variations in the molecular weights of the polyions involved, as well as their structures, functional groups, and the sizes of charged pendant chains and hydrogen bonding sites. However, quantifying the

effects of these latter components requires extensive investigation and cannot be fully explained based on the present work. The tensile strength of the membranes follows the decreasing order: LPV > PS-PV > LPD > PS-PD > LPU > Ionogel, with the strongest membranes resulting from the coatings of high molecular weight polyions (LPV and PV), while the lowest tensile strength is observed in the low molecular weight polycation (PU). These observations indicate that the molecular weight of the polyions significantly influences the tensile strength of the coated membranes; however, the effects of other structural parameters must be decoupled when drawing conclusions. Besides, the impact of molecular weight is somewhat less pronounced compared to electrostatic interactions. This LbL assembly not only enhances mechanical strength through robust electrostatic and hydrogen bonding interactions between polyions but also exhibits excellent elasticity, crucial for maintaining electrode contact and ensuring smooth battery operation under harsh conditions.

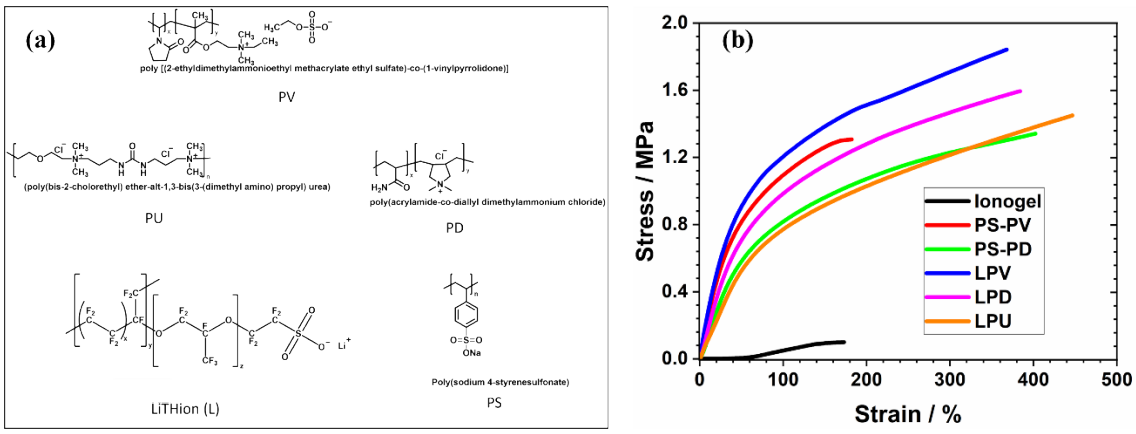

Figure 1. (a) Structure of polycations and polyanions used to prepare LbL assembly in ionogel; (b) Stress-strain plot of ionogel, PS-PV, PS-PD, LPV, LPD, LPU on a TA Q800 DMA analyzer using the controlled force method with a force ramp rate of 0.1 N/min.

Thermogravimetric analysis (TGA) (**Figure S1a**) illustrates the excellent thermal stability at high temperatures of both the ionogel and all LbL membranes. The decomposition temperature for all membranes is approximately 400 °C, indicating their robust thermal stability

suitable for high-temperature applications. Fourier-transform infrared spectroscopy (FT-IR) spectra (**Figure S1b**) show a decrease in the O-H stretching band (3600-3400 cm^{-1}), indicating enhanced hydrophobicity of the LbL membrane. SEM images of the LbL membranes reveal uniform distribution of polyions on the ionogel surface (top view, **Figures S2a**-low resolution, **S2b**-high resolution) and homogeneous distribution of the ionic liquid PVDF-co-HFP in cross-sectional views (cross-section, **Figure S2c**).

Temperature-dependent ionic conductivities of the original ionogel and LbL membranes were measured using broadband dielectric spectroscopy (BDS), with results shown in **Figure 2a**. The ionic conductivities of both ionogel and LbL membranes follow the Vogel–Fulcher–Tammann (VFT) behavior ($\sigma = \sigma_0 \exp(-B/(T - T_0))$), and their respective fitting parameters are tabulated in **Table S1**. As anticipated, all membranes exhibit increased ionic conductivities at higher temperatures. Apart from enhancing mechanical robustness, the LbL coating confines the ionic liquids within the ionogel matrix, thereby maintaining high ionic conductivities comparable to the original ionogel membranes. At 30 °C, the ionogel exhibited an ionic conductivity of 1.14×10^{-3} S cm^{-1}, while LbL coated membranes showed slightly lower values (PS-PV ~1.12×10^{-3} S cm^{-1}, PS-PD ~ 9.69×10^{-4} S cm^{-1}, LPV ~ 7.1×10^{-4} S cm^{-1}, LPD ~ 9.23×10^{-4} S cm^{-1}, LPU ~ 9.12×10^{-4} S cm^{-1}). It is noted that approximately 7-10 % weight loss of ionic liquids occurred during LbL coating, contributing to the slight decrease in ionic conductivities of LbL membranes. The VFT fitting of temperature-dependent ionic conductivities shows lower activation energies (**Table S1**), correlating with higher ionic conductivities. While the LbL membrane enhances mechanical strength and maintains ionic conductivities of the original ionogel, it does not improve the lithium-ion transport number (t_{Li}^+ for ionogel ~0.09 and LPV ~0.09; **Figure S3**). A high lithium-ion transport number is crucial for reducing polarization and achieving uniform current distribution, factors that mitigate

dendrite formation, even though the mechanical strength falls short (~1 GPa) of what is required to fully suppress dendrite growth.[56-58]

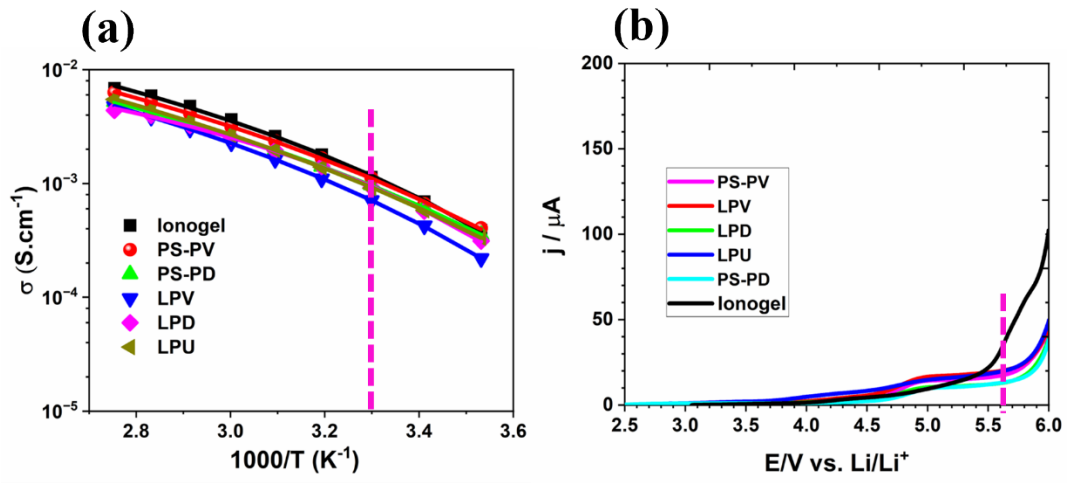

Figure 2. (a) Ionic conductivities of ionogel, PS-PV, PS-PD, LPV, LPD, LPU as a function of temperature; (b) Linear sweep voltammetry of a Li||Membrane||SS (stainless steel) cell with 10.00 mV s^{-1} applied potential at room temperature.

The oxidative stability of the LbL-membranes was assessed using LSV. **Figure 2b** displays the linear sweep voltammograms for both ionogel and LbL-coated membranes. In the ionogel, significant oxidation occurs beyond 5.5 V, whereas all LbL membranes show slightly improved oxidation stability, indicated by a substantial increase in oxidation current beyond 5.7 V. This enhanced stability in LbL membranes is attributed to the effective confinement of mobile anions within the polymer matrix, facilitated by strong coulombic interactions and hydrogen bonding among polyions.

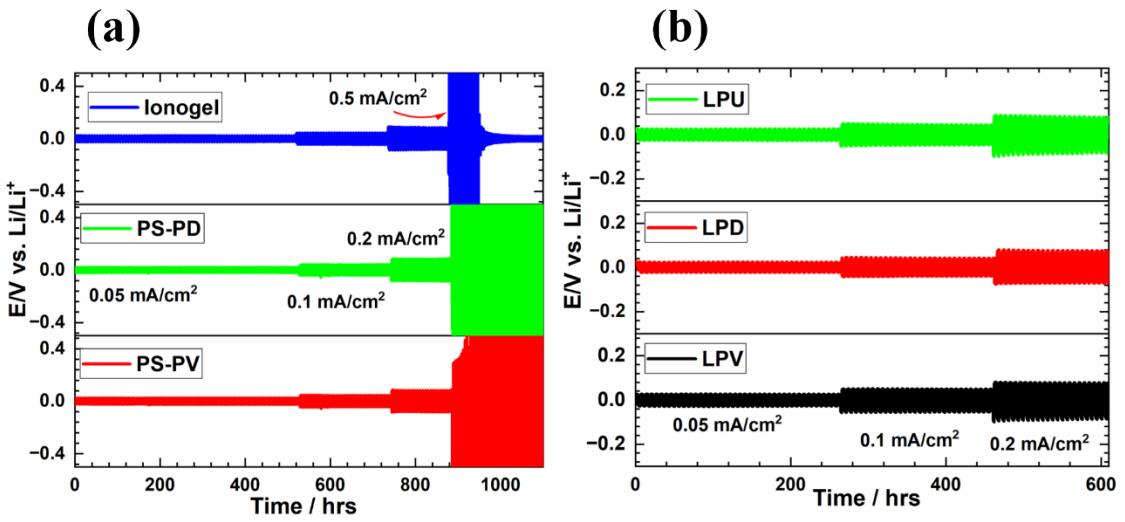

Figure 3. Comparison of Li metal plating/stripping performance for (a) Ionogel, PS-PV, and PS-PD; (b) LPV, LPD, and LPU at 60 °C at different current densities (50/100/200 μAcm^{-2}).

The interfacial compatibility and mechanical stability of LbL membranes in inhibiting lithium dendrite growth was investigated by conducting cycling tests of Li||LbL-membranes||Li symmetrical cells at 60 °C under various current densities (0.05/0.1/0.2/0.5 mA·cm^{-2}). Voltage profiles during Li metal plating/stripping for the ionogel and all LbL membranes are presented in **Figures 3a**, **3b**, and **Figure S4**. Across current densities of 0.05 to 0.2 mA·cm^{-2}, all membranes exhibited stable voltage profiles. However, at 0.5 mA·cm^{-2}, increased overpotential was observed in all membranes, likely due to slower lithium diffusion kinetics attributed to lower ionic conductivities. Notably, LbL membranes (PS-PV and PS-PD, **Figure 3a**) did not experience short circuiting, contrasting with ionogel which showed short circuiting after 900 hours. These findings suggest that LbL membranes possess superior mechanical robustness compared to ionogel, effectively suppressing dendrite growth over the testing duration. LPV, LPD, and LPU also demonstrated stable voltage profiles under the same conditions, underscoring the mechanical resilience of these membranes against lithium metal. Furthermore, in the extended voltage profiles presented in **Figure S4**, the high interfacial compatibility of LbL membranes was evident, complementing their mechanical strength.

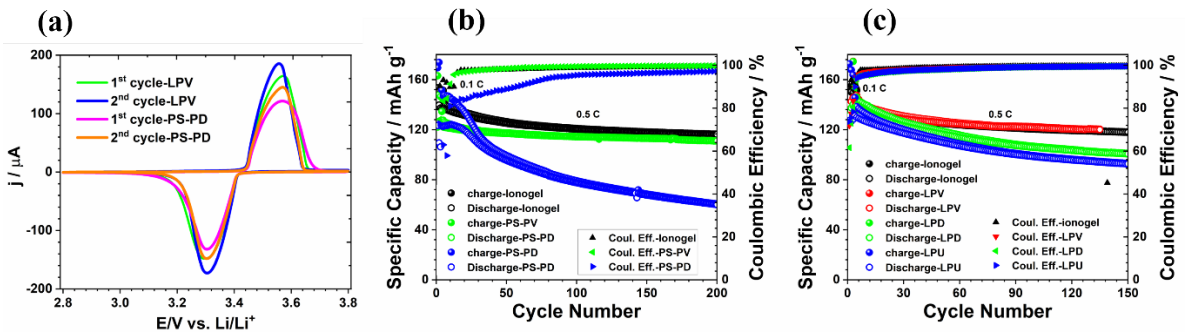

Figure 4. The electrochemical performance of Li||LbL-Membranes||LFP cell. (a) CV curve of LPV and PS-PV from 2.8 -3.8 V at a scan rate of 0.04 mV S^{-1}; Comparison of charge-discharge capacities and coulombic efficiencies of (b) Ionogel, PS-PV, PS-PD; and (c) Ionogel, LPV, LPD, LPU as a function of cycle number from 2.8 – 3.8 V at 0.1 C for first three cycles and 0.5 for the rest of the cycling period C at 60 °C (1C ~ 170 mAh g^{-1}).

The electrochemical performance of the LbL-membranes was evaluated in an all-solid-state coin cell setup (Li||LbL-membranes||LFP) utilizing lithium metal as the anode and LFP as the cathode, with ionogel or LbL-coated membranes serving as the solid electrolyte. The CV curves of the LbL membranes (LPV and PS-PV) paired with LFP cathodes (vs Li/Li^{+}) were recorded at a scan rate of 0.04 mV S^{-1}. **Figures 4a** and **S5** illustrate typical redox peaks for LFP cathodes, showing that both ionogel and LPV membranes exhibit similar CV curves with lower over potential (~ 60 mV), whereas PS-PD exhibits slightly larger overpotential (> 70 mV), indicating good lithium-ion diffusion kinetics through the membranes. **Figures 4b**, **4c, and S6** show the electrochemical performance of Li||LbL membranes||LFP cell at 60 °C at 0.1 C scan rate (1C = 170 mAh g^{-1}) for first three cycles and at 0.5 C scan rate for the remainder of the cycles reported here. **Figure S6(a & b** illustrate typical lithium de-/intercalation plateau for LFP cathodes at 0.1 C, showing that except PS-PD (~72 mV), all the membranes exhibit fairly lower overpotential (PS-PV~59 mV, LPV~60 mV, LPD~64 mV, and LPU~63 mV), comparable to ionogel (~60 mV) and other liquid electrolytes reported in literature.[59, 60] Such low overpotential suggests rapid lithium diffusion facilitated by good intrinsic ionic

conductivities due to decoupling of Li-ion from its counterions via strong coulombic interactions between polyions from LbL coatings.

Ionogel demonstrated a high first cycle coulombic efficiency (CE) of approximately 90%, whereas all LbL membranes showed lower first cycle CEs (<75%) (**Figure S6**), resulting in significant lithium inventory loss during the initial cycle. This diminished efficiency is attributed to parasitic side reactions at the electrode-electrolyte interface, leading to solid electrolyte interphase (SEI) formation, which reduces first cycle CE. The trapping of counterions during LbL assembly likely contributes to this phenomenon, as lower oxidative stability of these anions can promote oxidative parasitic reactions, SEI growth, and reduced CE. Consequently, due to lower first cycle CE and lithium loss, all LbL membranes exhibit rapid capacity decay. Ionogel retains approximately 76% of its capacity with an average CE of 99.92% after 200 cycles, starting from a first cycle CE of ~90% (First charge/discharge capacity ~153.7/138.5 mAh g^{-1} at 0.1 C). PS-PV and PS-PD show capacity retentions of ~68% and ~36% after 200 cycles, respectively, while LPV, LPD, and LPU exhibit capacity retentions of ~62%, 47%, and 54%, respectively (See **Table S2** for details). The coin cells utilizing LPV as an electrolyte exhibited reversible discharge capacities of approximately 120 mAh g^{-1} for LFP and around 165 mAh g^{-1} for NMC811 cathodes at room temperature. These capacities are slightly lower at a scan rate of 0.1 C compared to those at elevated temperatures (60 °C). Notably, the capacities dropped significantly when the rate increased to 0.3 C for the NMC811 cathode (to 84 mAh g^{-1}) but recovered to 166 mAh g^{-1} when cycled back to 0.1 C. Similarly, the LFP cathode delivered approximately 55 mAh g^{-1} at a rate of 0.5 C (see **Figure S7**). This behavior can likely be attributed to the lower intrinsic ionic conductivity of the membrane, a trend also observed in high-temperature experiments. Consequently, high-temperature electrochemistry was investigated to assess the suitability of these membranes for LMB applications in this work.

Despite demonstrating excellent Li-Li interfacial stability, good ionic conductivities, mechanical robustness, and fast lithium diffusion kinetics, the LbL membranes suffer from initial low CE (<75%), rendering them unsuitable for practical LMB applications. This issue is possibly due to incomplete ion exchange during LbL assembly and subsequent interfacial parasitic reactions, leading to uncontrolled SEI growth. This fact was further coroborated by X-ray photoelectron spectroscopy analysis of the cycled LFP electrode (see later). Addressing these challenges, particularly by ensuring complete removal of trapped counterions during LbL assembly, could potentially improve first cycle CE and reduce lithium inventory loss.

To validate this hypothesis, the LPV membrane was subjected to further treatment by soaking in a high concentration LiTFSI solution to remove trapped counterions. LPV was selected based on its superior mechanical strength and initial electrochemical performance compared to other LbL membranes. The treatment involved soaking LPV in a 5 M LiTFSI solution for an hour, followed by drying at 110°C for 3 weeks. The resulting treated LPV membrane is referred to as T-LPV hereafter. Due to concentration gradient of LiTFSI in solution and membrane, LiTFSI flux directed towards the membrane via osmosis, and removed trapped counterions in membrane. It is important to note that approximately 54% of the IL was leached from the membrane during the scrubbing process, and a corresponding 132% increase in the weight of LiTFSI was observed. This corresponds to an approximately fourfold increase in the molal concentration of LiTFSI compared to the original LPV membrane. The duration of soaking can impact the membrane's electrochemical performance and should be optimized based on final ionic conductivities and membrane flexibility for future applications.

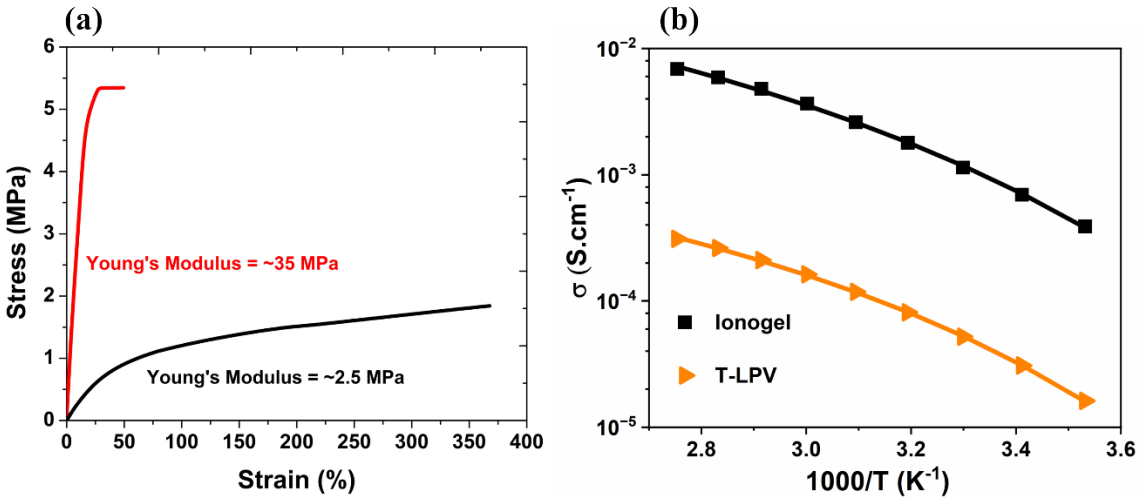

Figure 5. (a) Stress-strain plot of LPV (black curve) and T-LPV (red curve) on a TA Q800 DMA analyzer using the controlled force method with a force ramp rate of 0.1 N/min; (b) Ionic conductivities of LPV and T-LPV as a function of temperature.

SEM images of T-LPV showed no significant changes post-treatment compared to the LbL membrane before treatment (**Figures S8a**, **S8b**, and **S8c**). The mechanical strength and ionic conductivity of T-LPV, crucial for LMBs, were evaluated prior to further electrochemical analysis. The mechanical strength of T-LPV (**Figure 5a**) significantly improved (Young's modulus ~ 35 MPa) compared to the pretreated LPV (~ 2.5 MPa). However, T-LPV exhibited reduced elasticity and flexibility relative to LPV, likely due to increased LiTFSI concentration during soaking. This trend was mirrored in the ionic conductivity of T-LPV (5.2×10^{-5} S cm^{-1} at 30 °C, **Figure 5b**), which decreased substantially compared to pretreated LPV (7.1×10^{-4} S cm^{-1}), attributed to the loss of ILs, coupled with the increase in LiTFSI content post-treatment, significantly reduced the membrane's elasticity and flexibility, thereby impeding Li-ion mobility.[61]

The enhanced mechanical strength and improved lithium-ion transference number (t_{Li}^{+}) from 0.09 (LPV, **Figure S3**) to 0.37 (LPV, **Figure S9**) following treatment indicated increased LiTFSI diffusion into the membrane due to concentration gradients. The T-LPV membrane

exhibits stable voltage profiles during cycling in the Li||T-LPV||Li symmetrical cell at 60 °C (**Figure S10**), indicating robust interfacial compatibility with lithium. However, it displays a slightly higher overpotential compared to the Li||LPV||Li configuration (**Figure 3b**). This increased overpotential can be attributed to the lower ionic conductivity of the T-LPV membrane. These enhancements are advantageous for the cycling stability of LMBs. Electrochemical performance of T-LPV in Li||T-LPV||LFP coin cells at 60 °C was compared with ionogel. A minimal amount of EC/EMC was used to soak LFP cathode before cell assembly to improve interfacial contact between the membrane and LFP cathode.

Figure 6a shows the charge-discharge capacities and CE of T-LPV in an all pseudo-solid-state cell configuration (Li||T-LPV||LFP) over 400 cycles. T-LPV exhibited initial charge/discharge capacities of 162.9/162.02 mAh g^{-1} with a first cycle CE of ~ 99.4% (**Figure 6b**), significantly outperforming ionogel (153.7/138.6 mAh g^{-1}, CE ~ 90.1%, **Figure 6c**). The voltage profiles indicated comparable lithium-ion diffusion kinetics at the membrane interface, with slightly higher overpotentials for T-LPV (63 mV) compared to ionogel (60 mV) during initial cycles. Notably, T-LPV maintained a stable overpotential of 78 mV after 399 cycles, contrasting with overpotential of ionogel increase to 148 mV, suggesting superior interfacial stability and compatibility of T-LPV that mitigated side reactions and enhanced electrochemical performance.

After 400 cycles, the LFP cell with T-LPV membrane sustained a stable capacity of ~142 mAh g^{-1} with a capacity retention (CR) of ~87%, corresponding to a decay rate of 0.03 % per cycle with average CE of ~ 99.6 %. In contrast, the LFP cell with ionogel showed a capacity of ~112 mAh g^{-1} with a CR of ~73%, corresponding to a decay rate of 0.06 % per cycle with average CE of ~ 99.3 %. These findings underscore the significant improvement in electrochemical performance facilitated by the post-treatment of the LbL membrane for LMB applications.

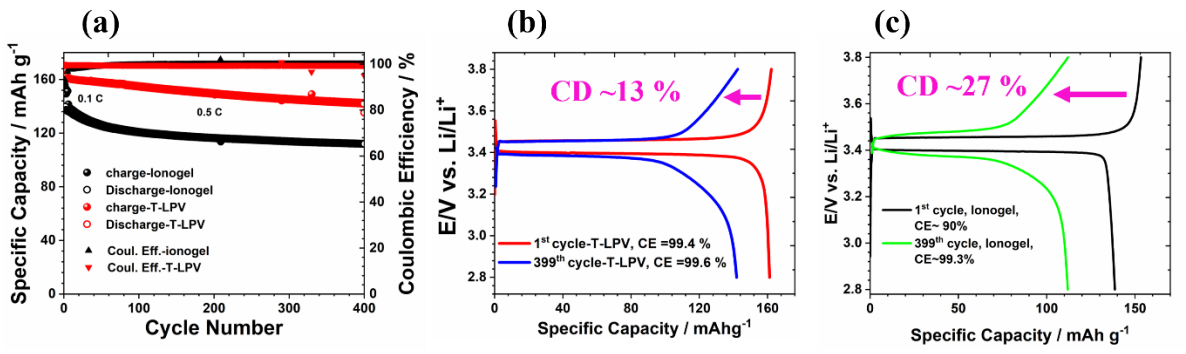

Figure 6. (a) Comparison of specific (charge-discharge) capacities and coulombic efficiencies of LFP cathode with Ionogel, and T-LPV as a solid electrolyte as a function of cycle number from 2.8 – 3.8 V at 0.1 C for first three cycles and 0.5 C for the rest of the cycling period at 60 °C; Comparison of the 1st and 399th charge-discharge voltage profiles of (b) T-LPV, and (c) ionogel.

The T-LPV membrane served as a solid electrolyte in conjunction with a Li||T-LPV||NMC811 ($LiNi_{0.8}Mn_{0.1}Co_{0.1}O_2$) cathode system. Electrochemical performance evaluation of the NMC811 cathode was conducted within a voltage range of 3-4.4 V, initially at a scan rate of 0.1 C for three cycles, followed by 0.3 C for subsequent cycles (1C = 200 mAh g^{-1}) at an elevated temperature of 60 °C (refer to **Figure 7**). The first cycle charge/discharge capacity of the NMC811 cathode was approximately 233/208 mAh g^{-1} with a CE of about 89% (see **Figure 7b**). After 85 cycles, it retained a specific capacity of around 149.0 mAh g^{-1} with an average CE exceeding 99.9%. The electrochemical performance of T-LPV was comparable to that of NMC811 when using the baseline electrolyte (1.2 M LiPF6 in EC-EMC, 3:7 volume ratio) (**Figure S11a**). Notably, the first-cycle coulombic efficiency (CE) and average CE of the NMC811 cell with T-LPV were significantly superior compared to the baseline electrolyte, which yielded a first-cycle CE of 87.7% (first charge/discharge capacity of approximately 231.58/203.07 mAh g^{-1}) and an average CE of about 98.5%. It is important to note that the electrochemical performance of NMC811 with the baseline electrolyte was evaluated at room temperature. The NMC811 cell exhibited good rate capabilities across varying rates from 0.1

C to 5C and demonstrated recovery to its initial capacity upon returning to 0.1 C cycling, indicative of the membrane's stable interfacial behavior and mechanical robustness (refer to **Figure 7c**). At lower current rates (0.1–0.5 C), both electrolytes (T-LPV and baseline) delivered similar specific capacities. However, at higher current rates, the T-LPV electrolyte exhibited a slightly reduced capacity compared to the baseline electrolyte, with the difference in capacities becoming more pronounced as the current rate increased from 1 C to 5 C. This reduction is likely due to the lower intrinsic ionic conductivity of T-LPV (**Figure S11b**). These results underscore the potential of T-LPV as a pseudo-solid electrolyte for lithium metal batteries (LMBs).

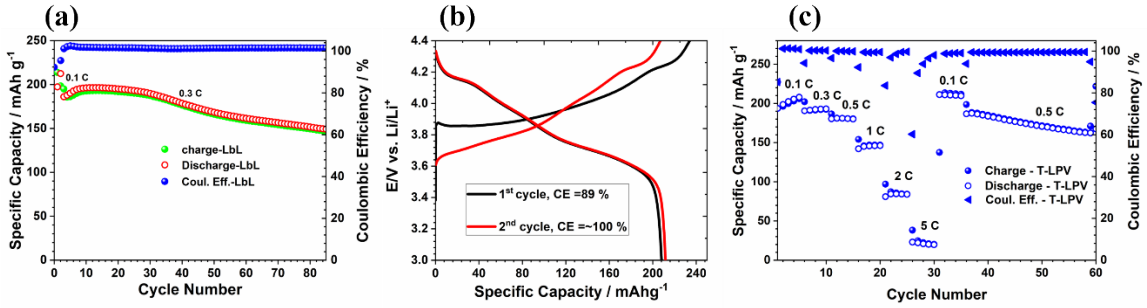

Figure 7. (a) Showing specific (charge-discharge) capacities and coulombic efficiencies of NMC811 with T-LPV as electrolyte as a function of cycle number from 3.0 – 4.4 V at 0.1 C for first three cycles and 0.3 C for the rest of the cycling period at 60 °C; (b) 1st and 2nd charge-discharge profiles at 0.1 C rate; (c) Charge-discharge capacities and coulombic efficiencies at different scan rate from 0.1 – 5 C.

To confirm that the SEI growth, driven by parasitic side reactions at the electrode-electrolyte interface, is the primary reason for the low first-cycle CE, X-ray photoelectron spectroscopy (XPS) was conducted on cycled Li||LPV||LFP, Li||T-LPV||LFP, and Li||T-LPV||NMC811 electrodes after the first charge-discharge cycles. The thickness and composition of the interphase layer on the cycled Li||LPV||LFP and Li||T-LPV||LFP electrodes are presented in **Figure S12(a-e)**, with a wide energy spectrum shown in **Figure S13**. The C 1s

spectrum (**Figure S12c**) of the cycled Li||LPV||LFP electrode reveals the presence of CF_x, -CO_3, O=C-O, C=O, C-O, and C-C species, with a more complex overlap between species compared to the Li||T-LPV||LFP cell. The F 1s spectra (**Figure S12e**) displayed similar amounts of C-F species; however, the Li||T-LPV||LFP electrode contained significantly fewer Li-F species. This was further substantiated by the depth profiles (**Figures S12a** and **S12b**), which indicate a higher concentration of Li-F species in the Li||LPV||LFP cells. Additionally, the N 1s spectra showed the presence of nitrite species (**Figure S12d**) in Li||LPV||LFP cells, whereas these species were absent in Li||T-LPV||LFP cells. The thickness of the interphase layer was determined by depth profiling through Ar-etching, where 5 seconds of Ar-etching was estimated to correspond to ~1 nm of depth. The continuous increase in the Li signal and decrease in the F signal suggest that the interphase layer in Li||LPV||LFP cells grows consistently during galvanostatic cycling, reaching a thickness of over 30 nm. In contrast, the interphase growth in Li||T-LPV||LFP cells becomes nominal beyond ~6 nm, as indicated by minimal changes in the Li and F signals.

This XPS analysis confirms that the low first-cycle CE observed for LbL membranes is primarily due to uncontrolled parasitic reactions, which are mitigated after post-treatment. The T-LPV membrane exhibited significantly improved CE. Similar results were observed in the Li||T-LPV||NMC811 cells, where the interphase layer thickness was approximately 3 nm (**Figure S14**). These findings corroborate the excellent electrochemical performance of the Li||T-LPV||NMC811 cells.

This study illustrates that the LbL assembly of polyions on ionogel enhances mechanical strength, reduces the leakage of ionic liquids, and maintains ionic conductivity. The conformal coating of oppositely charged polymers creates strong electrostatic interactions, thereby improving mechanical strength without compromising the liquid-like conducting behavior of ionic liquids. Furthermore, the study identifies that the mechanical and electrochemical

properties are influenced by the pendant groups. The type, size, and location of charged groups within the pendant chains significantly influence the mechanical and electrochemical properties of the membranes. For instance, polycations such as PV, which contain methacrylate, pyrrolidone, and quaternary ammonium groups, exhibit superior mechanical strength and electrochemical performance compared to other polycations, such as PD and PU. This is due to the longer pendant chains with quaternary ammonium cationic groups in PV, which alleviate steric hindrance between polyion chains, resulting in stronger Coulombic interactions and higher tensile strength.

Similarly, the location of amine groups also affects mechanical strength through hydrogen bonding. For example, the -NH_2 group in the pendant chain of PD can readily form hydrogen bonds with oppositely charged polyions, whereas the -NH group in the backbone of PU experiences steric hindrance, preventing strong hydrogen bonding. Consequently, LPU exhibits lower mechanical strength compared to LPD. However, further investigation is needed to decouple the effects of each parameter and quantitatively assess their individual contributions to the mechanical and electrochemical properties.

Mechanical characterization demonstrates that all LbL-coated membranes exhibit enhanced mechanical robustness compared to uncoated ionogel. However, achieving sufficient mechanical strength alone does not mitigate dendrite growth. Addressing this challenge could be enhanced by selecting polyions with varied pendant groups containing different functional moieties, capable of anchoring negatively charged anions to decouple lithium ions. This approach not only enhances mechanical strength but also improves lithium-ion transference number, thereby reducing polarization and further suppressing dendrite growth. These promising findings suggest that the LbL approach holds potential to address issues associated with gel electrolytes, transforming them into pseudo-solid membranes. However, optimizing mechanical strength and electrochemical performance is crucial to resolve safety concerns in practical applications of LMBs.

3. Conclusion

In conclusion, we have successfully developed a highly charged polyelectrolyte membrane through the sequential deposition of polyions onto a neutral ionogel membrane. Our approach leverages the inherent ionic structure of ionogels for facile interface modification. The LbL polyelectrolytes exhibit enhanced mechanical strength and electrochemical stability, rendering them suitable for high-voltage applications and improving electrochemical performance. A detailed investigations highlighted the significant influence of functional groups on pendant chains on mechanical and electrochemical properties. Symmetric Li||Li cell cycling demonstrates robust interfacial compatibility and effective suppression of lithium dendrites. Following optimization, the LbL membrane (T-LPV) exhibits significantly enhanced electrochemical performance when paired with an LFP cathode, achieving approximately 162.9 / 162 mAh g^{-1} charge / discharge capacity, with a first-cycle Coulombic efficiency of approximately 99.4% and maintaining around 87% capacity after 400 cycles, equivalent to a minimal capacity loss of 0.03% per cycle. Similarly, T-LPV shows promising performance with a high-capacity, high-voltage NMC811 cathode, delivering 233/208 mAh g^{-1} charge / discharge capacity and a first-cycle Coulombic efficiency of approximately 89%. These findings underscore the potential of LbL-assembled ionogel membranes as compelling pseudo-solid electrolytes for the development of robust and a commercially viable all solid-state LMBs with higher battery efficiency and safety.

4. Experimental Section/Methods

Materials and Methods: Poly(sodium 4-styrenesulfonate) solution (PS, M_w ~ 1,000,000, Sigma-Aldrich), poly(vinylidene fluoride-*co*-hexafluoropropylene) (PVDF-*co*-HFP, M_w ~ 400,000, M_n ~ 130,000, Sigma-Aldrich), 1-methylpyrrolidine (>98%, Sigma-Aldrich), 1-bromobutane (99%,

Sigma-Aldrich), poly (acrylamide-co-diallyldimethylammonium chloride) (PD, $M_W \sim 250{,}000$, Sigma-Aldrich), lithium bis(trifluoromethanesulfonimide) (LiTFSI, >99%, Sigma-Aldrich). LITHion (10 wt. % aqueous solution, ion power sources, exact molecular weight not provided), poly [(2-ethyldimethylammonioethyl methacrylate ethyl sulfate)-co-(1-vinylpyrrolidone)] (PV, 20 wt. % aqueous solution, $M_W < 1{,}000{,}000$, Sigma Aldrich), and ((poly(bis-2-cholorethyl) ether-alt-1,3-bis(3-(dimethylamino) propyl) urea) quaternized (PU, 62 wt.% aqueous solution, $M_W > 10{,}000$, Sigma-Aldrich) were used as received for the LbL membrane fabrication.

Procedures for the synthesis of ionic liquid-1-butyl-1-methylpyrrolidinium bis(trifluoromethanesulfonimide): Ionic liquid 1-butyl-1-methylpyrrolidinium bis(trifluoromethanesulfonimide) (BMPyTFSI) was synthesized following the published procedure.[31, 34, 62]

Procedures for the fabrication of ionogels: The solid composite polymer electrolyte membranes were produced using a conventional solvent casting method. A solution containing 20 wt. % PVDF-co-HFP and 80 wt. % 0.5 m LiTFSI/BMPy-TFSI in acetone was prepared. The solution was drop-cast onto a glass Petri dish and allowed to slowly evaporate the solvent over 24 hours at room temperature, resulting in homogeneous composite films of the desired thickness. Subsequently, residual solvent and moisture were eliminated by heating the films at 100 °C in a vacuum oven for 24 hours. These membranes were designated as "ionogel".

Procedures for LbL coating of polyanions and polycations: The ultrathin coating of polyanions and polycations was achieved using a LbL assembly technique. Initially, the ionogel was immersed in a 0.1 wt. % solution of either polycations such as poly(bis-2-cholorethyl) ether-alt-1,3-bis(3-(dimethyl amino) propyl) urea (PU), poly[(2-ethyldimethylammonioethyl methacrylate ethyl sulfate)-co-(1-vinylpyrrolidone)] (PV), or poly(acrylamide-co-diallyl dimethylammonium chloride) (PD) for 20 seconds. Subsequently, the membrane underwent a washing step with deionized water to remove loosely bound polymer chains. After air-drying, it was immersed in a 0.1 wt. % solution of polyanions such as poly(sodium 4-styrenesulfonate)

(PS) or Lithion (L) for 20 seconds, followed by another washing step to eliminate loosely attached polymers. This layering process was repeated for 25 cycles. The outermost layer of the membrane consisted of polyanionic polymers (either PS or L) (see **Seheme 1**). The membrane was then dried in a vacuum oven at 120°C for three weeks to remove residual water and stored in an argon-filled glove box with moisture and oxygen contents below 0.5 ppm. The resulting LbL membranes were designated as "PS-PV" and "PS-PD" if the outer layer was PS, and "LPV", "LPD", or "LPU" if the outer layer was L. Additionally, LPV membranes underwent immersion in a 5 M LiTFSI aqueous solution for 1 hour to remove residual counterions from the polyelectrolyte coating, followed by extensive drying under vacuum at 120°C for three weeks, referred to as treated LPV (T-LPV).

Membrane Characterization: Mechanical strength characterization of the bulk films involved tensile testing using a dynamic mechanical analyzer (DMA Q800) with a rectangular membrane (~4.0 mm × ~3.0 mm). Stress-strain analysis was conducted in controlled force mode at 25 °C with a force ramp rate of 0.1 N min^{-1}. Infrared spectra (IR) of ionogel and LbL membranes were acquired using a Nicolet IS50 FT-IR (ATR) spectrometer spanning 4000-500 cm^{-1}. Surface morphology examination was performed via scanning electron microscopy (SEM).

Electrochemical Measurements: Ionic conductivity of of ionogels and LbL membranes were measured employing an Alpha-A analyzer from Novocontrol in the frequency range of 10^{-1} Hz to 10^{6} Hz. A hermetic cell configuration included a cap as a bottom electrode and an upper electrode separated by a sapphire window to prevent electrical contact. Samples, cut into circles with a 10 mm diameter, were placed between the electrodes in the dielectric cell. The standard calibration procedure was used. The samples were measured with applied AC voltage of 0.1 V. Temperature control during measurements was achieved using a Novocontrol Quattro temperature controller, stabilizing each temperature for 15 minutes to ensure a ±0.2 K variation.

The electrochemical potential stability window was evaluated via linear sweep voltammetry (LSV), scanning from 2.0 V to 6.0 V vs. Li/Li^+ at a scan rate of 10 mV s^{-1} using Li||ionogel or LbL membranes||stainless steel (SS) cells. Compatibility and interfacial stability against lithium were assessed using symmetric Li||ionogel or LbL membranes||Li cells assembled in an argon-filled glove box (moisture and oxygen < 0.5 ppm).The lithium transference number(t_{Li+}) was calculated using the following equation involving dc polarization and ac impedance impedance[31] measurements of symmetric Li||ionogel or LbL membranes||Li cells.

$$t_{Li+} = [I_s\ (_{\Delta}V\text{-}I_iR_i)]/[I_i\ (_{\Delta}V\text{-}I_sR_s)]$$

where $_{\Delta}V$ is the polarization bias voltage, I_i , R_i, and I_s , R_s are initial and steady-state currents and resistance, respectively.

The stability of lithium-membrane interfaces was investigated through lithium stripping-plating cycles on symmetric Li||ionogel or LbL membranes||Li cells, operating periodically under specified charge and discharge conditions (3 hours charge, 1 hour rest followed by 3 hours discharge and 1 hour rest). Electrodes for LFP and NMC811 cathodes were prepared by casting a homogeneous slurry of LFP or NMC811, carbon black (CB 45), and PVDF in N-methyl-pyrrolidone (NMP) onto aluminum foil, followed by drying under vacuum at 110 °C. The weight ratio of LFP (or NMC811), CB45, PVDF was 70:20:10 (90:05:05 for NMC811). Circular discs with electrode surface areas of 1.27 cm^2 and active mass loadings of ~1.0-1.3 mg cm^{-2} for LFP, and ~6 mg cm^{-2} for NMC811, were punched out. All electrochemical tests were conducted in 2032-type coin cells assembled with lithium anodes, LFP/NMC811 cathodes, and ionogel/LbL membranes as electrolytes and separators in an argon-filled glove box (oxygen and moisture < 0.5 ppm). Battery performance testing was carried out using an Arbin Battery testing instrument, with cyclic voltammetry (CV) performed on a bio-logic VSP instrument. Galvanostatic charge-discharge cycles for LFP were executed over a voltage range

of 2.8 V–3.8 V at a scan rate of 0.1 C for the initial three cycles and 0.5 C at 60 °C, while CV scans were collected from 2.8 V–3.8 V at a scan rate of 0.04 mV s^{-1}. Similarly, galvanostatic charge-discharge cycles for NMC811 were performed over a voltage range of 3.0 V–4.4 V at a scan rate of 0.1 C for the initial three cycles and 0.3 C at 60 °C.

Supporting Information

Supporting Information is available from the Wiley Online Library or from the author.

Notes

The authors declare no competing financial interest.

Acknowledgements

This work was supported by the U.S. Department of Energy, Office of Science, Office of Basic Energy Sciences, Materials Sciences and Engineering Division under contract number DE-AC05-00OR22725 with the US Department of Energy (DOE). The conductivity measurements were supported by the National Science Foundation (award CHE-2102425).

Received: ((will be filled in by the editorial staff))
Revised: ((will be filled in by the editorial staff))
Published online: ((will be filled in by the editorial staff))

References

[1] M. S. Whittingham, *Chemical Reviews* **2004**, *104*, 4271-4302.

[2] T. Kim, W. Song, D.-Y. Son, L. K. Ono, Y. Qi, *Journal of Materials Chemistry A* **2019**, *7*, 2942-2964.

[3] J. M. Tarascon, M. Armand, *Nature* **2001**, *414*, 359-367.

[4] M. Armand, J. M. Tarascon, *Nature* **2008**, *451*, 652-657.

[5] A. Manthiram, *ACS Central Science* **2017**, *3*, 1063-1069.

[6] J. Zhang, Y. Bai, X.-G. Sun, Y. Li, B. Guo, J. Chen, G. M. Veith, D. K. Hensley, M. P. Paranthaman, J. B. Goodenough, S. Dai, *Nano Letters* **2015**, *15*, 3398-3402.

[7] A. Mauger, C. M. Julien, J. B. Goodenough, K. Zaghib, *Journal of The Electrochemical Society* **2020**, *167*, 070507.

[8] H. G. Lee, S. Y. Kim, J. S. Lee, *npj Computational Materials* **2022**, *8*, 103.

[9] J. Janek, W. G. Zeier, *Nature Energy* **2016**, *1*, 16141.

[10] S. Yu, S. Schmohl, Z. Liu, M. Hoffmeyer, N. Schön, F. Hausen, H. Tempel, H. Kungl, H. D. Wiemhöfer, R. A. Eichel, *Journal of Materials Chemistry A* **2019**, *7*, 3882-3894.

[11] A. Manthiram, X. Yu, S. Wang, *Nature Reviews Materials* **2017**, *2*, 16103.

[12] J. Janek, W. G. Zeier, *Nature Energy* **2023**, *8*, 230-240.

[13] B. M. Wiers, M.-L. Foo, N. P. Balsara, J. R. Long, *Journal of the American Chemical Society* **2011**, *133*, 14522-14525.

[14] Y. Liu, L. Hou, Y. Jiao, P. Wu, *ACS Applied Materials & Interfaces* **2021**, *13*, 13319-13327.

[15] C. Cho, F. Xiang, K. L. Wallace, J. C. Grunlan, *Macromolecules* **2015**, *48*, 5723-5729.

[16] S. Devasahayam, C. M. Hussain, *Sustainable Materials and Technologies* **2020**, *26*, e00233.

[17] C. A. Nguyen, A. A. Argun, P. T. Hammond, X. Lu, P. S. Lee, *Chemistry of Materials* **2011**, *23*, 2142-2149.

[18] X. Han, Y. Gong, K. Fu, X. He, G. T. Hitz, J. Dai, A. Pearse, B. Liu, H. Wang, G. Rubloff, Y. Mo, V. Thangadurai, E. D. Wachsman, L. Hu, *Nature Materials* **2017**, *16*, 572-579.

[19] Y. Ren, T. Liu, Y. Shen, Y. Lin, C.-W. Nan, *Ionics* **2017**, *23*, 2521-2527.

[20] J. Wan, J. Xie, X. Kong, Z. Liu, K. Liu, F. Shi, A. Pei, H. Chen, W. Chen, J. Chen, X. Zhang, L. Zong, J. Wang, L.-Q. Chen, J. Qin, Y. Cui, *Nature Nanotechnology* **2019**, *14*, 705-711.

[21] S. Li, S.-Q. Zhang, L. Shen, Q. Liu, J.-B. Ma, W. Lv, Y.-B. He, Q.-H. Yang, *Advanced Science* **2020**, *7*, 1903088.

[22] X. Yu, A. Manthiram, *Energy Storage Materials* **2021**, *34*, 282-300.

[23] C. A. Angell, C. Liu, E. Sanchez, *Nature* **1993**, *362*, 137-139.

[24] A. M. Christie, S. J. Lilley, E. Staunton, Y. G. Andreev, P. G. Bruce, *Nature* **2005**, *433*, 50-53.

[25] M. Irfan, M. Atif, Z. Yang, W. Zhang, *Journal of Power Sources* **2021**, *486*, 229378.

[26] Q. Zhou, J. Ma, S. Dong, X. Li, G. Cui, *Advanced Materials* **2019**, *31*, 1902029.

[27] Y. An, X. Han, Y. Liu, A. Azhar, J. Na, A. K. Nanjundan, S. Wang, J. Yu, Y. Yamauchi, *Small* **2022**, *18*, 2103617.

[28] J. Le Bideau, L. Viau, A. Vioux, *Chemical Society Reviews* **2011**, *40*, 907-925.

[29] S. Zekoll, C. Marriner-Edwards, A. K. O. Hekselman, J. Kasemchainan, C. Kuss, D. E. J. Armstrong, D. Cai, R. J. Wallace, F. H. Richter, J. H. J. Thijssen, P. G. Bruce, *Energy & Environmental Science* **2018**, *11*, 185-201.

[30] Y. Zhang, Z. Zheng, X. Liu, M. Chi, Y. Wang, *Journal of The Electrochemical Society* **2019**, *166*, A515.

[31] B. P. Thapaliya, I. Popov, S. Dai, *ACS Applied Energy Materials* **2020**, *3*, 1265-1270.

[32] Z. Wang, B. P. Thapaliya, I. Popovs, Y. Wang, T. Wang, J. Chen, M. A. Arnould, S. M. Mahurin, S. Dai, *ACS Applied Materials & Interfaces* **2023**, *15*, 51806-51814.

[33] L. Han, M. L. Lehmann, J. Zhu, T. Liu, Z. Zhou, X. Tang, C.-T. Heish, A. P. Sokolov, P. Cao, X. C. Chen, T. Saito, *Frontiers in Energy Research* **2020**, *8*.

[34] B. P. Thapaliya, C.-L. Do-Thanh, C. J. Jafta, R. Tao, H. Lyu, A. Y. Borisevich, S.-z. Yang, X.-G. Sun, S. Dai, *Batteries & Supercaps* **2019**, *2*, 985-991.

[35] J.-F. Wu, X. Guo, *Small* **2019**, *15*, 1804413.

[36] A. Manuel Stephan, K. S. Nahm, *Polymer* **2006**, *47*, 5952-5964.

[37] J. Fu, J. B. Schlenoff, *Journal of the American Chemical Society* **2016**, *138*, 980-990.

[38] P. T. Hammond, *Advanced Materials* **2004**, *16*, 1271-1293.

[39] G. Decher, *Science* **1997**, *277*, 1232-1237.

[40] N. Joseph, P. Ahmadiannamini, R. Hoogenboom, I. F. J. Vankelecom, *Polymer Chemistry* **2014**, *5*, 1817-1831.

[41] M. Cui, W. S. Ng, X. Wang, P. Darmawan, P. S. Lee, *Advanced Functional Materials* **2015**, *25*, 401-408.

[42] K. Ariga, J. P. Hill, Q. Ji, *Physical Chemistry Chemical Physics* **2007**, *9*, 2319-2340.

[43] Y. Li, X. Wang, J. Sun, *Chemical Society Reviews* **2012**, *41*, 5998-6009.

[44] J. Borges, J. F. Mano, *Chemical Reviews* **2014**, *114*, 8883-8942.

[45] R. R. Costa, J. F. Mano, *Chemical Society Reviews* **2014**, *43*, 3453-3479.

[46] G. Rydzek, Q. Ji, M. Li, P. Schaaf, J. P. Hill, F. Boulmedais, K. Ariga, *Nano Today* **2015**, *10*, 138-167.

[47] T. Lee, S. H. Min, M. Gu, Y. K. Jung, W. Lee, J. U. Lee, D. G. Seong, B.-S. Kim, *Chemistry of Materials* **2015**, *27*, 3785-3796.

[48] D. M. DeLongchamp, P. T. Hammond, *Chemistry of Materials* **2003**, *15*, 1165-1173.

[49] D. M. DeLongchamp, P. T. Hammond, *Langmuir* **2004**, *20*, 5403-5411.

[50] A. A. Argun, J. N. Ashcraft, P. T. Hammond, *Advanced Materials* **2008**, *20*, 1539-1543.

[51] O. S. Sakr, G. Borchard, *Biomacromolecules* **2013**, *14*, 2117-2135.

[52] V. Kozlovskaya, S. A. Sukhishvili, *Macromolecules* **2006**, *39*, 5569-5572.

[53] E. Kharlampieva, S. A. Sukhishvili, *Langmuir* **2004**, *20*, 9677-9685.

[54] S. Y. Yang, J. D. Mendelsohn, M. F. Rubner, *Biomacromolecules* **2003**, *4*, 987-994.

[55] J. D. Rule, E. N. Brown, N. R. Sottos, S. R. White, J. S. Moore, *Advanced Materials* **2005**, *17*, 205-208.

[56] Y. Zhong, J. Zhang, S. Wang, D. Han, M. Xiao, Y. Meng, *Materials Advances* **2020**, *1*, 873-879.

[57] X. Zhou, X. Li, Z. Li, H. Xie, J. Fu, L. Wei, H. Yang, X. Guo, *Journal of Materials Chemistry A* **2021**, *9*, 18239-18246.

[58] Y. Xia, P. Zhou, X. Kong, J. Tian, W. Zhang, S. Yan, W.-h. Hou, H.-Y. Zhou, H. Dong, X. Chen, P. Wang, Z. Xu, L. Wan, B. Wang, K. Liu, *Nature Energy* **2023**, *8*, 934-945.

[59] A. Guerfi, M. Dontigny, P. Charest, M. Petitclerc, M. Lagacé, A. Vijh, K. Zaghib, *Journal of Power Sources* **2010**, *195*, 845-852.

[60] C. Liao, X.-G. Sun, S. Dai, *Electrochimica Acta* **2013**, *87*, 889-894.

[61] G. A. Giffin, *Nature Communications* **2022**, *13*, 5250.

[62] A. K. Burrell, R. E. D. Sesto, S. N. Baker, T. M. McCleskey, G. A. Baker, *Green Chemistry* **2007**, *9*, 449-454.

The conformal coating of functionally tailored polyions on a neutral ionogel via layer-by-layer (LbL) assembly improves the mechanical strength and electrochemical performances without affecting ionic conductivities.

Bishnu P. Thapaliya[1*], *Babafemi Adigun*[2], *Tao Wang*[1], *Md Dipu Ahmed*[2], Harry M. Meyer III,[1] *Ivan Popov*[2,3], *Sheng Dai*[1,2*]

Mechanically Reinforced Pseudo-Solid Polyelectrolyte Membranes Via Layer-by-Layer Assembly for High-Performing Lithium Metal Batteries